



Characterization of contact properties in biocemented sand using 3D X-ray micro-tomography

Abdelali Dadda¹ · Christian Geindreau¹ · Fabrice Emeriault¹ · Sabine Rolland du Roscoat¹ · Annette Esnault Filet² · Aurélie Garandet³

Received: 23 January 2018 / Accepted: 15 October 2018 / Published online: 25 October 2018
© Springer-Verlag GmbH Germany, part of Springer Nature 2018

Abstract

The mechanical efficiency of the biocementation process is directly related to the microstructural properties of the biocemented sand, such as the volume fraction of calcite, its distribution within the pore space (localized at the contact between grains, over the grain surfaces) and the contact properties: coordination number, contact surface area, contacts orientation and types of contact. In the present work, all these micromechanical properties are computed, for the first time, from 3D images obtained by X-ray tomography of intact biocemented sand samples. The evolution of all these properties with respect to the volume fraction of calcite is analyzed and compared between each other (from untreated sand to highly cemented sand). Whatever the volume fraction of calcite, it is shown that the precipitation of the calcite is localized at the contacts between grains. These results are confirmed by comparing our numerical results with analytical estimates assuming that the granular medium is made of periodic simple cubic arrangements of grains and by considering two extreme cases of precipitation: (1) The calcite is localized at the contact, and (2) the grains are covered by a uniform layer of calcite. In overall, the obtained results show that a small percentage of calcite is sufficient to get a large amount of cohesive contacts.

Keywords Biocementation · Contact orientation · Contact surface area · Coordination number · MICP · X-ray micro-tomography

1 Introduction

Strong interactions between the geotechnical engineering and the biology these recent years have resulted in the discoveries of different natural processes, which can be transformed into soil reinforcement techniques such as the biocementation by using catalytic microorganisms and the bioclogging for water filtrations, which can be performed by pore-filling material generated by microbial processes [20]. The microbial-induced calcite precipitation (MICP) is considered as one of the most promising techniques of

biocementation. Hence, several research works have been performed in order to evaluate the efficiency of this technique for different geotechnical problems in the laboratory by performing standard geotechnical tests [2, 4–7, 11, 13, 14, 18, 19, 28] and in situ by achieving large-scale tests [17, 27]. Almost all of these studies have shown that this technique strongly enhances the mechanical properties of the soil and slightly decreases the transfer properties such as permeability [8].

Most of these studies [2, 6] also point out that the mechanical efficiency of this process is directly related to the microstructural properties changes of the sand induced by the biocementation process (precipitation manner of calcite inside the sand specimen and size of calcite crystals), which are mainly controlled by the treatment conditions: concentrations of bacteria, calcification solution; and the in situ conditions: water content, particle size and distribution, temperature, etc. [2, 6].

✉ Abdelali Dadda
Abdelali.dadda@3sr-grenoble.fr

¹ CNRS, GINP, Laboratoire Sols, Solides, Structures et Risques (3SR), Université Grenoble Alpes, Grenoble, France

² Soletanche Bachy, Rueil-Malmaison, France

³ Compagnie Nationale du Rhône, Lyon, France

Two precipitation scenarios have been discussed in previous works:

- **The localized precipitation:** In that case, the calcite precipitates preferentially in the grain contacts zone and increases the cohesion of the soil significantly, with a slight modification of the friction angle. The part of calcite which forms a bridge between two grains is called the effective part (active calcite). This configuration or precipitation manner is the most common one which has been observed by using scanning electron microscope [9, 22, 23, 26]. This affinity of precipitating in particle-to-particle contacts has been described by DeJong et al. [9] using two parameters: the biological behavior and filtering process. During the biocementation process, the bacteria prefers to get attached in the grain contact zones, because of the weak shear stress of fluid flow and the availability of nutriment in these specific places (biological behavior). The other amount of bacteria is suspended in pore fluid, and the calcification occurs in this place. Thus, small crystals are suspended and are then forced by the injection process to be attached near the region of intergranular contacts (filtering process). Controlling the amount of effective calcite is possible in reinforced soils by controlling the soil saturation during the biocementation process. Cheng et al. [6] have shown that lower saturation states have provided more resistant specimens compared to higher saturated specimens due to the localization of the calcite in the small meniscus of water (intergranular contacts).
- **Uniform precipitation:** In that case, the calcite is deposited uniformly on the soil grains and increases slightly the intergranular contact surface area which causes a slight increase in cohesion and friction angle. In that case, a large amount of the calcite are considered as passive because it is not contributing in the cohesion evolution, but it is contributing in an indirect way to the mechanical strength, by roughening the grain surfaces and increasing the friction angle of the treated soil. The surface roughness is an important parameter in the friction angle evolution but not the only one, and other parameters interact between each other's such as the effective particle size distribution after cementation, the effective angularity and the coordination number.

Concerning the size of calcite crystals, Al Qabany and Soga [1] have recently shown that this parameter has a slight influence on the unconfined compression strength. More precisely, they have shown that smaller calcite crystals obtained by low concentration of reactants give slightly higher mechanical resistance compared to a biocemented sand, which contains larger calcite crystals obtained with high chemical reactants concentrations.

Clearly, the mechanical efficiency of the biocementation process is directly related to the microstructural properties of the biocemented sand, such as the calcite volume fraction and its distribution within the pore space (at the contact between grains, at the surfaces of the grains), the coordination number, the contact surface area and the contact orientation. Nowadays, X-ray micro-tomography represents one of the most efficient techniques to explore the 3D microstructural properties of a porous media in qualitative and quantitative ways. The accuracy of the results depends on the resolution and the contrast of the objects in the 3D images [24]. Different studies have been performed to follow the contact characteristics during in situ tests using X-ray observations [3, 10, 12]. Andò [3] has performed in situ triaxial tests on sand and has extracted the evolution of the contact parameters for different triaxial stress levels by separating in two different ways the grains in the 3D images, and by computing the evolution of the contacts surface area and the coordination number. In this work, the resolution was not sufficient to capture the punctual contact between two grains, and the contact surface area have been quantified by direct counting of voxels, which can result in some errors. Tageliaziri et al. [25] have performed in situ triaxial test on biocemented sand with X-ray micro-tomography observations. In this work, the chosen resolution of $(15 \mu\text{m})^3/\text{voxel}$ was not sufficient to capture the shape and the distribution of the calcite at the pore scale. Recently, 3D images of some biocemented samples were performed using X-ray synchrotron micro-tomography on the ID19 beamline at the ESRF in Grenoble [8]. A resolution of $(0.65 \mu\text{m})^3/\text{voxel}$ was chosen in order to visualize precisely the calcite crystals, which have a typical size of 10 micrometers. After thresholding, the trinarized images were used to compute mean microstructural properties (porosity, volume fraction of calcite, specific surface area, etc.) and to quantify their impact on some transport properties (permeability, effective diffusion tensor, etc.) according to the level of biocementation.

In the present work, we propose to determine and to quantify the evolution of the contact properties (contact surfaces, coordination number, contacts orientation, type of contact, etc.) of biocemented sand as function of the cementation level using 3D images obtained by X-ray micro-tomography. The numerical results computed on representative elementary volumes extracted from the 3D images are then compared with numerical values obtained on simple periodic arrangements (SC) of sand grains, assuming that the precipitation is localized at the contacts between grains or uniform. The present paper is organized as follows. Section 2 is devoted to the materials and methods: 3D images treatment, computed contact properties (coordination number, contact surface area, contact

orientation and type of contact). In Sect. 3, the properties computed from the 3D images are presented, discussed and compared with analytical estimates on simple microstructures (SC), with a uniform or a localized precipitation.

2 Materials and methods

2.1 Sample preparation

Different biocemented subsamples have been extracted from triaxial specimens of biocemented sand (Table 1). These triaxial specimens have been prepared using Fontainebleau sand (NE34) with an initial porosity ranging from 37 to 40%. The mean diameter of sand grains is $D_{50} = 0.21$ mm with a uniformity coefficient $C_u = 1.5$. The sand has been prepared inside plastic columns with diameter of 68 mm and different lengths (340 and 560 mm). These columns have been firstly flushed with commercial water (Cristaline water) in order to be saturated. Then, two solutions have been injected successfully for the biocementation process inside these columns from the bottom to the top: (1) bacterial solution which contains one optical density (1 OD₆₀₀) of *S. pasteurii* provided under a dried form by Soletanche Bachy (Soletanche Bachy Entreprise, Rueil-Malmaison, France) with 3 g of sodium chloride (NaCl) dissolved in one liter of commercial water, in order to increase potential attachment of bacteria to soil grains and (2) reactants solution (calcifying solution) which contains 1.4 mol of urea and the same amount of calcium chloride. These operations have been repeated one or more time in order to obtain different biocementation levels (see Dadda et al. [8], for more details).

2.2 Image acquisition

As already mentioned, 3D images of these biocemented samples were performed using X-ray synchrotron microtomography with a resolution of $(0.65 \mu\text{m})^3/\text{voxel}$ on the ID19 beamline at the ESRF (Grenoble, France). As already mentioned, this resolution has been chosen in order to

visualize precisely the calcite crystals, which have a typical size of 10 micrometers. Moreover, the field of view is $(3250 \times 3250 \times 2000 \text{ voxels})$, i.e., $(2.11 \times 2.11 \times 1.3 \text{ mm}^3)$ to obtain 3D images large enough to be representative of the material (Dadda et al. [8]).

2.3 Image treatments

To compute the microstructural properties linked to the contact, the 3D images must be treated in order to (1) identify the three phases (pores, sand and calcite), (2) to separate and label the grains, which constitute the (sand + calcite) phase and (3) to identify and label the contacts between grains.

2.3.1 Identification of three phases (pore, sand, calcite)

After reconstruction, 3D images in gray levels represent a 3D map that is proportional to the density of each phase within the scanned sample. In order to compute microstructural quantities, the 3D images in gray levels (Fig. 1—A1) have been treated to separate the three phases (pore, sand and calcite). In the present case, the pore and the solid (sand + calcite) phases were easily separated by a simple thresholding [21]. By contrast, the separation of the calcite and sand phases was not straightforward, because of the similar density of these two constituents (for the sand $\rho_s = 2650 \text{ kg/m}^3$, for the calcite $\rho_c = 2710 \text{ kg/m}^3$). To overcome this problem, a Gaussian distribution of the gray level of both phases has been assumed to define the second threshold by symmetry (between sand and calcite) (see Dadda et al. [8] for more details). Fig. 1—A3 shows a 2D image of the sample ‘113MB’ after treatment, where we can distinguish the three phases: pore in light gray, sand in orange and calcite in purple.

2.3.2 Grains separation and labeling

The second step of this image processing consists in the separation of the grains, which constitute the (sand + calcite) phase. This operation has been performed on binarized 3D images of biocemented sand, i.e., assuming that the sand and calcite phases have the same gray level (Fig. 1—image A2), using the software Visilog[®]. Particle separation is obtained using a 3D watershed algorithm. The particle labeling was then achieved with Matlab[®] by detecting the grains in the 3D images. The key parameter of this watershed is the tolerated intensity variation to group the markers of the objects in 3D. Indeed, this parameter controls directly the final number of grains. In the biocemented sand, the surfaces of grains are rough, which can lead to an over separation of the grains if this

Table 1 Characteristics of the scanned subsamples. (Dadda et al. [8])

Subsample	2T	12MB	13TT	11BB	13BT	13MB
Volume fraction of calcite f_c (%)	1.9	3.2	4.7	6.2	8.8	14.8
Calcite m_c (% in mass)	3	5	7	9	12.7	16.9
Initial porosity ϕ_0	40	40	38	38	37	38

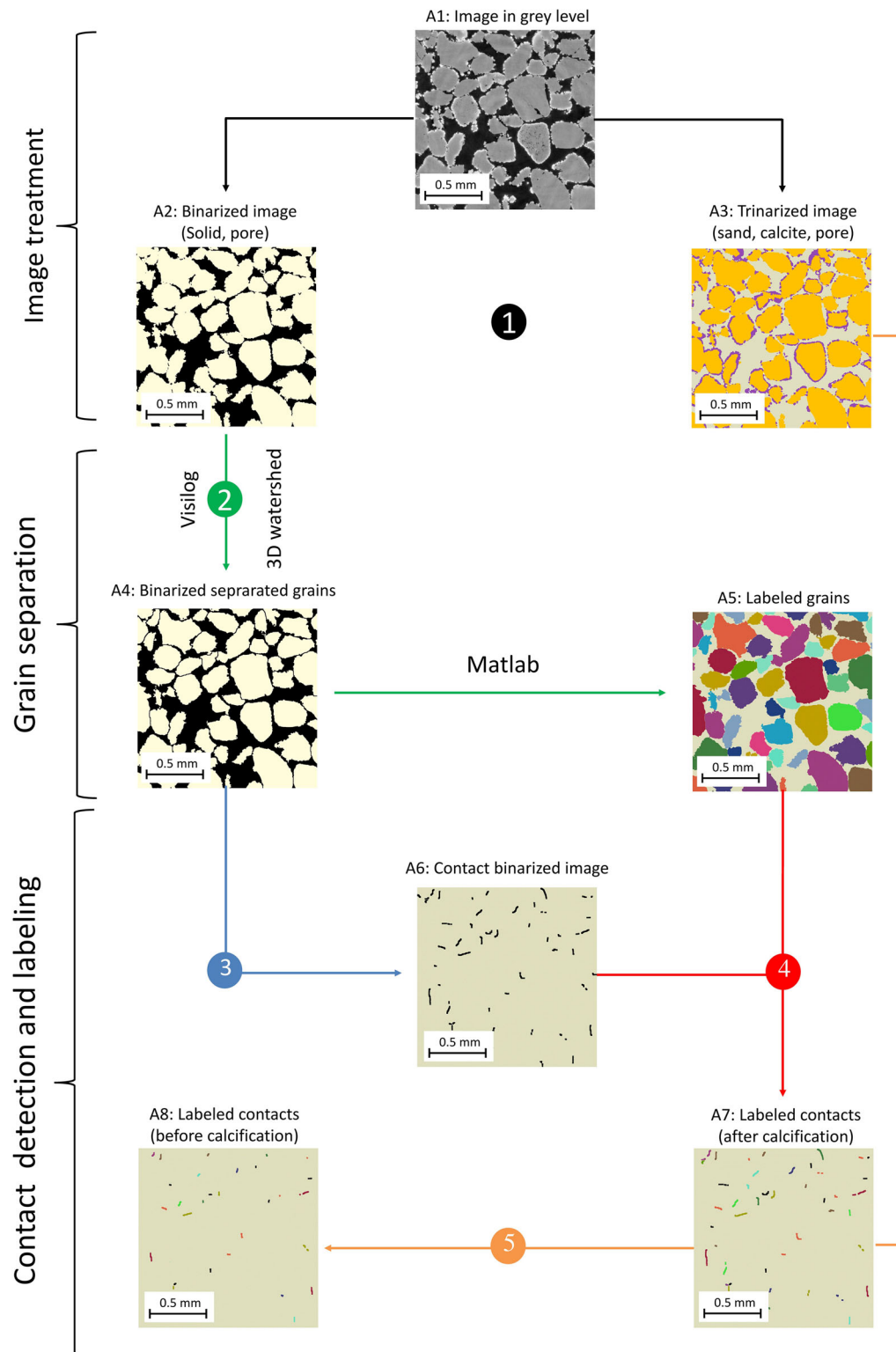


Fig. 1 Different steps of the image treatment (subsample '13BT')

parameter is too small. In the present work, several attempts have been performed on the 3D images in order to determine the optimal value leading to realistic grain separation. An optimal value of 8 was found. For example, the

image A5 (Fig. 1) corresponds to the image A2 where the grains (sand + calcite) are now separated and labeled by using different color levels. The contact between two

grains is characterized by a voxel cloud with a width of one voxel.

Finally, let us remark, for each biocemented subsample, a similar 3D image containing the sand grains only, which can be obtained by removing the calcite phase identified on the 3D image A3 from the image A5. This image is considered as the initial state of the sand before calcification for each subsample.

2.3.3 Identification of each contact and labeling

In order to identify and label each contact, a dedicated routine has been developed in Matlab[®]. All the contact surfaces (Fig. 1—image A6) are computed by subtracting the image A2 and the image A4 (Fig. 1). Then, the Matlab routine allows labeling all the contacts between grains by following a method similar to the one developed by Andô [3]. This method consists in scanning the 26 neighbor voxels of each voxel of the contact surfaces (image A6) and in determining the minimum and the maximum color level of these neighbor voxels in the labeled grains image (image A5). All the voxels with the same minimum and maximum color levels are then supposed to constitute one surface of contact between the two grains labeled with the minimum and maximum color levels, respectively. If the maximum and minimum color levels are equal, which can occur due some artifacts induced by the grains separation process (voxel of a contact surface inside a grain, for example), the voxel is deleted. The image A7 (Fig. 1) corresponds to the image A6 after the labeling of all the contacts.

As previously, the 3D image of the labeled contacts without calcite (Fig. 1—A8) is then obtained by removing the calcite phase identified on the image A3 from the image A7.

2.4 Computed contact properties

2.4.1 Coordination number

From both images A5 and A7 (Fig. 1), a list of all the labeled grains with their corresponding contacts can be constructed. From this list, the coordination number (Z_i) of each grain ' i ' can be easily computed. Figure 2c shows the distribution of the coordination number (the number of contacts per grains) computed on the 3D image of size ($1.3 \times 1.3 \times 1.3 \text{ mm}^3$), which contains around 700 grains (Fig. 2a), before and after biocementation. According to these results, we can observe that many grains present 1–4 contacts only with the others, which is unrealistic. These grains correspond to the ones located close to the edges of the image. In order to avoid this 'edge effects,' all these grains (around 300), in black on Fig. 2b, have not been

taken into account in the following analysis. Figure 2d presents the new distribution of the coordination number of the grains within the sample. This distribution has a classical Gaussian shape. From this distribution, for each sample, we can compute the mean coordination number \bar{Z} and the total number of contact n_t , before (noted with a subscript 'b') and after (noted with a subscript 'a') the biocalcification. For the sample '13MB' presented on Fig. 2, we have typically: $n_{tb} = 798$, $\bar{Z}_b = 7.7$ and $n_{ta} = 809$, $\bar{Z}_a = 7.8$.

2.4.2 Contact surface area

A cloud of voxels with a complex 3D shape (inclined rough surface) represents each contact surface between two grains (Figs. 3b, c). A direct computation of the voxels number can be used as a first estimation of the contact surface area. However, this method usually underestimates the real value. For that reason, different methods (marching cube, voxel-based area estimation, Crofton method, etc.) have been proposed in order to compute the surface area of a cloud of voxels [15, 16]. In this work, all the contact surface areas have been estimated by using the Matlab function 'geometric measures in 2D/3D images' developed by Legland et al. [15]. The surface area is measured using a discretization of the Crofton formula. For regular 3D objects (cubes, spheres and plane surfaces), a discretization along the three main orthogonal directions is sufficient to get a good accuracy of the surface area. When the surface is irregular with a complex shape, it has been shown that 13 directions of discretization are sufficient to estimate the surface area with accuracy [15]. In order to evaluate the errors induced by the method, the surface area of well-known surfaces have been computed. The surfaces under consideration are planar square surfaces of different sizes (the number of voxels varies between 100 and 10,000, i.e., the area ranges between 50 and 5000 μm^2 that are typical values encountered in the samples) inclined with an angle of 45° with respect to both planes (XY) and (XZ). An error has been found ranging from 3% for the small surfaces to 15% for the larger ones.

For example, Fig. 3d presents the distribution of the contact surface area for the subsample '13MB,' before and after biocalcification. From these results, we can compute the total contact surface area S_t within the sample and the mean contact surface area of each contact defined as $\bar{S} = S_t/n_t$. The total cohesive (or calcite) contact surface area noted as S_{tc} is obtained by subtracting to the contact surface area after calcification S_{ta} the one before calcification S_{tb} : $S_{tc} = S_{ta} - S_{tb}$. The mean cohesive (calcite) contact surface area (\bar{S}_c) per contact is given by $\bar{S}_c = S_{tc}/n_{ta}$. For the subsample '13MB,' we have typically $S_{tb} = 4.3 \times 10^5 \mu\text{m}^2$,

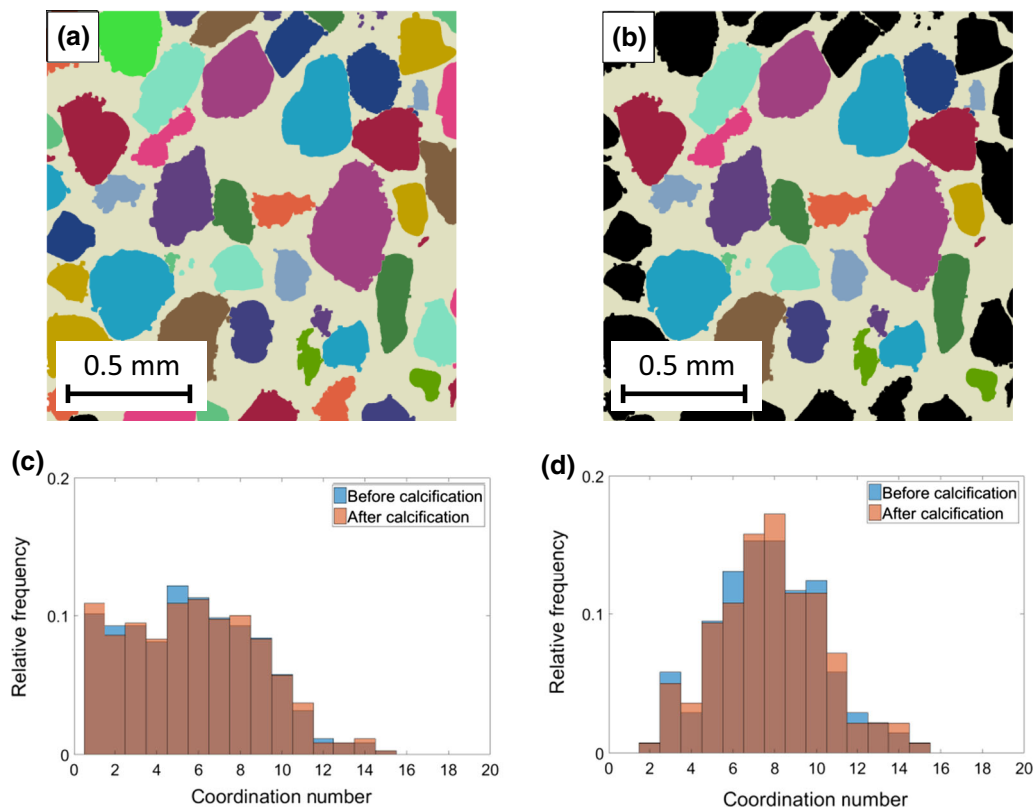


Fig. 2 Distribution of the coordination numbers (c) within the image (a) before and after biocementation, distribution of the coordination numbers (d) within the image (b) before and after biocementation, without ‘edge effects’ (subsample ‘13MB’)

$S_{ta} = 10^6 \mu\text{m}^2$, $S_{tc} = 5.7 \times 10^5 \mu\text{m}^2$, $\bar{S}_b = S_{tb}/n_{tb} = 564 \mu\text{m}^2$, $\bar{S}_a = S_{ta}/n_{ta} = 1237 \mu\text{m}^2$ and $\bar{S}_c = S_{tc}/n_{ta} = 705 \mu\text{m}^2$. In the present case, the mean contact surface area after biocementation is more than 2 times larger than the one before biocementation.

2.4.3 Identification of contact types

The type of contact in soil micromechanics is a very important parameter to understand and to predict the macro-mechanical behavior of soils. Generally, in untreated saturated sand, the contacts between two grains of silica are ‘frictional.’ After cementation, we can distinguish three different types of contact: (1) ‘frictional’ contacts (silica only) as in untreated sand (Fig. 4a), (2) ‘mixed’ contacts (Fig. 4b) and (3) ‘cemented’ contacts (Fig. 4c). ‘Mixed’ contacts are ‘frictional’ contacts which became ‘cohesive’ due to the biocalcification process, as illustrated in Fig. 4. ‘Cemented’ contacts are new contacts created by a bridge of calcite between two grains (Fig. 5). A Matlab[®] routine has been developed in order to determine these different contacts in each sample, by scanning the constituent (calcite and/or sand) of each contact surface using images A3 and A7 (Figs. 1, 4).

Figure 5a shows, for example, the distribution associated with the number of contacts within the subsample 13MB. The number of ‘frictional,’ ‘mixed’ and ‘cemented’ contacts is noted as n_{af} , n_{am} and n_{ac} , respectively, with $n_{ta} = n_{af} + n_{am} + n_{ac}$. In the present case, $n_{af} = 91$, $n_{am} = 707$ and $n_{ac} = 11$. This distribution is not enough to evaluate the efficiency of the process; the distribution associated with the surface area of each type of contact is also very important. Figure 5b presents such distribution within the sample 13MB. The total surface area associated with each type of contact is noted as S_{af} , S_{am} and S_{ac} , with $S_{ta} = S_{af} + S_{am} + S_{ac}$. For the subsample 13MB, we have: $S_{af} = 8 \times 10^4 \mu\text{m}^2$, $S_{am} = 9.6 \times 10^5 \mu\text{m}^2$ and $S_{ac} = 2.1 \times 10^4 \mu\text{m}^2$. In the present case, we can observe that most of the contacts after biocementation are ‘mixed’ contacts. Some ‘frictional’ contacts remain, and very few ‘cemented’ contacts are created.

2.4.4 Contact orientation

A cloud of voxels characterizes each contact between two grains. In order to determine the orientation of each contact, this cloud of voxels has been fitted (mean square method) by the equation of a plane in 3D. The normal of this plane, which represents the contact orientation, is then

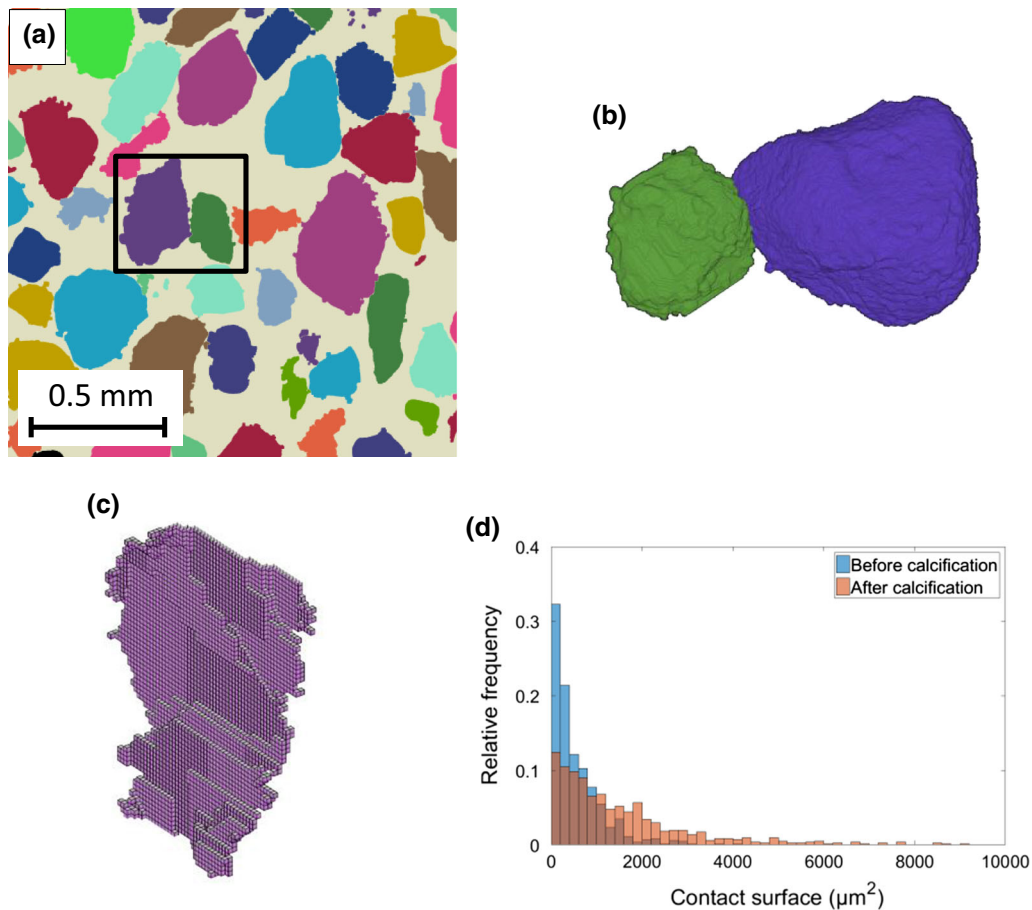


Fig. 3 Geometry of the grain to grain contacts: **(a)** 2D labeled grains image, **(b)** example of two grains in contact, **(c)** contact surface between the two grains in contact, **(d)** distribution of the contact surface area before and after calcification (subsample ‘13MB’)

computed. In the following, \mathbf{p}_i is the unit vector associated with the contact ‘ i .’ These orientations have been computed for the contacts within the sample before and after biocalcification. In a fixed orthonormal coordinate system, the vector \mathbf{p}_i can be defined by its polar angle θ $[0, 2\pi]$ and its azimuthal angle φ $[0, \pi]$. Figure 6 presents the polar orientation of all the contacts with the sample 13MB, before and after biocalcification. Different colors are used to distinguish the orientation of the ‘frictional’ contacts (in blue), the ‘mixed’ contacts (in red) and the ‘cemented’ contacts (in green). In the present case, we can observe that the contacts within the sample, before and after biocalcification, are not oriented in a privileged direction, and almost all the ‘frictional’ contacts before biocalcification became ‘mixed’ contact after biocalcification. This later result is consistent with the one presented in Fig. 5.

Using these results, we can also compute the fabric tensor (\mathbf{A}^c) associated with the contacts orientation and defined as: $[\mathbf{A}^c] = \sum_N \mathbf{p}_i \otimes \mathbf{p}_i$, where N ($= n_{ta}$, or n_{tb}) is the total of contacts under consideration. Figure 6 presents the matrix associated with \mathbf{A}^c in the principal axis. We can

observe that the diagonal values are close to 0.33, which confirms that the contact orientation within the subsample ‘13MB’ before and after biocalcification is isotropic.

3 Result and discussion

3.1 Coordination number

Figure 7a presents the distribution of the coordination number within the six samples under consideration, before and after biocalcification. This figure shows that whatever the volume of calcite, the distribution has a Gaussian shape. When the volume fraction of calcite increases, the distribution after biocalcification slightly moves to the right, i.e., the number of contacts per grain slightly increases due to the calcification process. This result is confirmed by Fig. 8 which presents the evolution of the ratio (\bar{Z}_a/\bar{Z}_b) of the mean coordination number after and before biocalcification with respect to the volume fraction of calcite. Let us remark that the initial mean coordination number \bar{Z}_b of all the specimen is about (7.1–8.5) depending

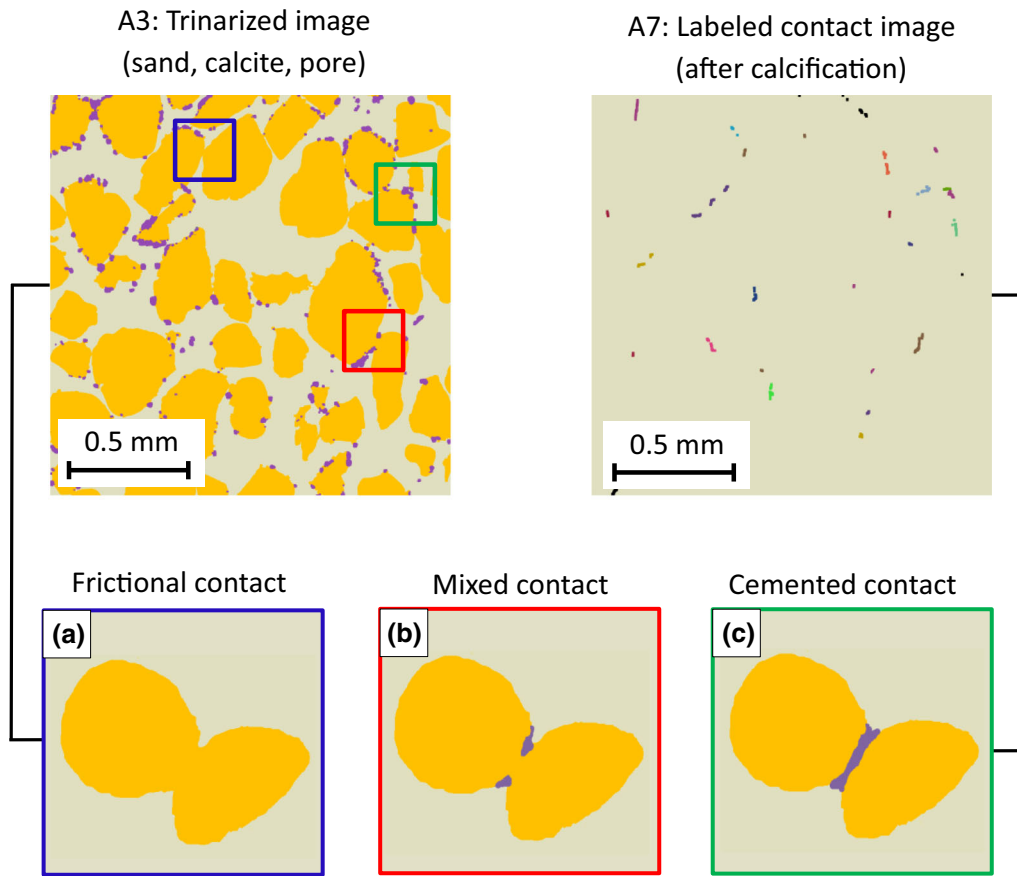


Fig. 4 Definition of the different types of contact

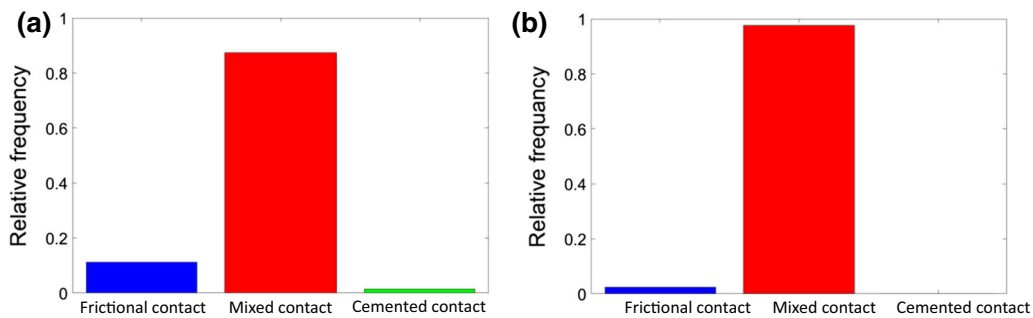


Fig. 5 Distribution of the different types of contact. **a** Number of contacts, **b** contact surface area (subsample ‘13MB’)

on the initial porosity ϕ_0 which varies between 37 and 40% (see Table 1). This ratio (\bar{Z}_a/\bar{Z}_b) is almost constant and equal to 1 when the volume fraction of calcite is lower than 3.2% and then increases nonlinearly until 1.08 for a volume fraction of calcite equal to 14.8%. As expected, due to the calcification process, new contacts or calcite bridges between grains are created. Even if this increase of the mean coordination number is moderate, it can affect significantly the macroscopic behavior of the sample, such as the shear strength. This increase could be higher in the case

of loose soils, where the coordination number before calcification is lower.

3.2 Contact surface area

Figure 7b shows the distribution of contact surface areas before and after calcification for the six specimens. Before biocalcification, as expected, the contact surface areas are small. For all the samples, these contact surface areas typically range between 0 and 3000 μm^2 , and more than

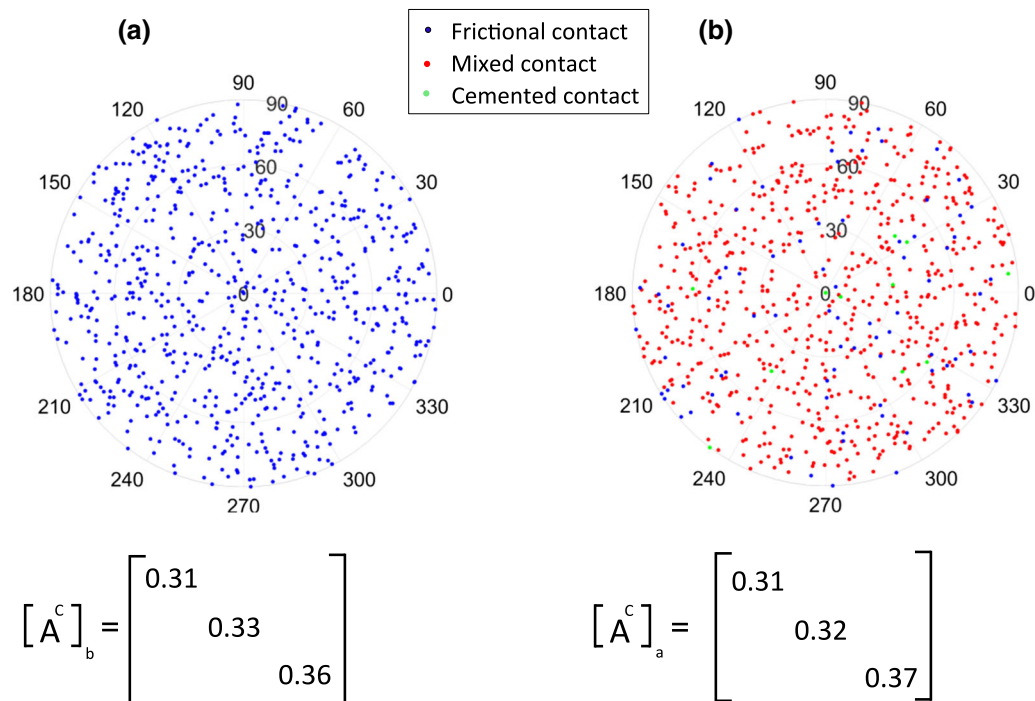


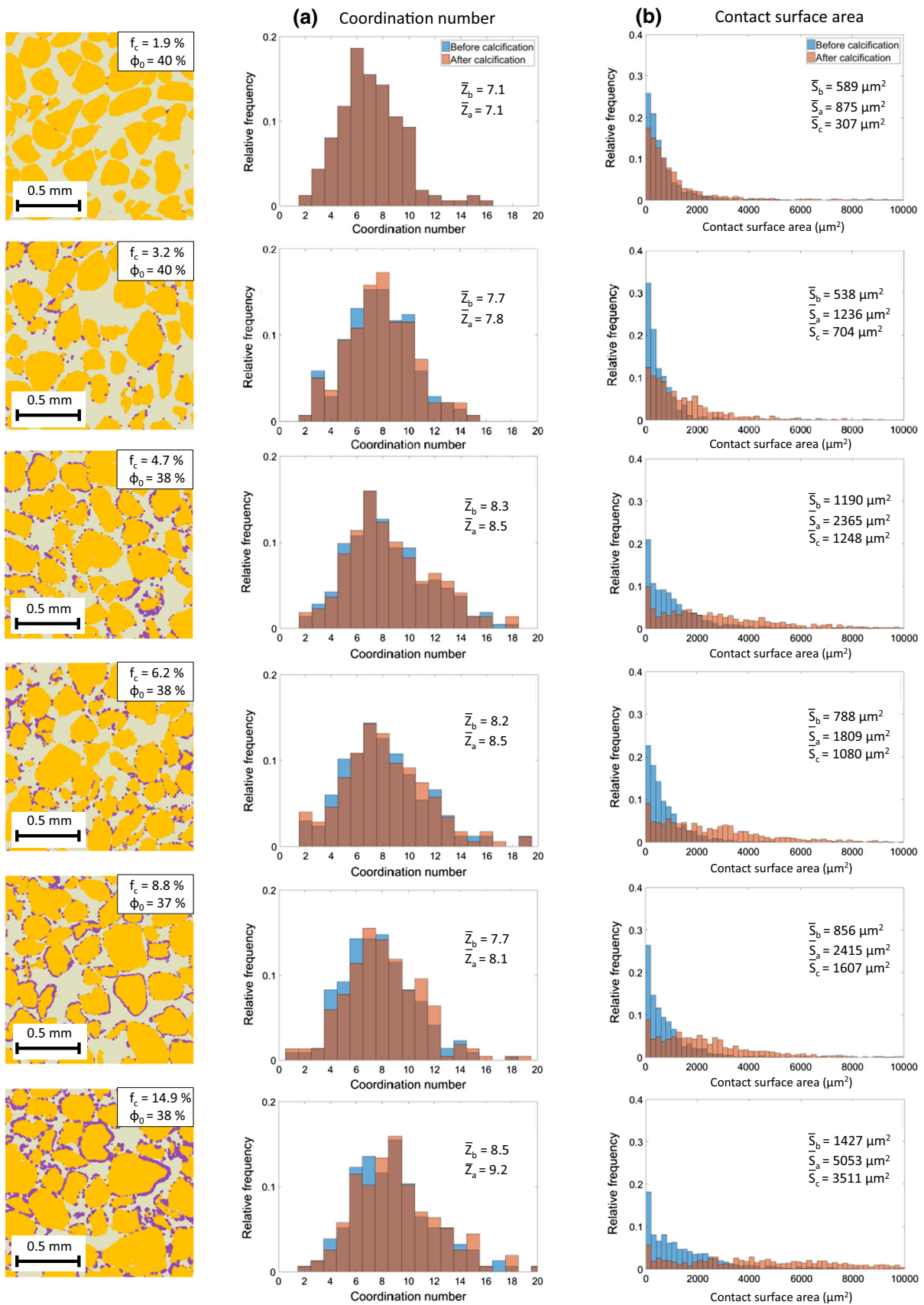
Fig. 6 Contact orientation before (a) and after (b) biocalcification (subsample ‘13MB’)

50% of these contact surfaces are smaller than $600 \mu\text{m}^2$, which represents less than 0.4% of the typical outer surface of a grain ($S_{D50} = 14 \times 10^4 \mu\text{m}^2$ with $D_{50} = 210 \mu\text{m}$). These small values of contact surface area before calcification are due to the nature of contacts between grains in 3D which are almost punctual. After biocalcification, Fig. 7b clearly shows that the distribution of contact surface areas changes progressively as function of the volume fraction of calcite. Indeed, the small surfaces are progressively transformed into large surfaces. The distribution of the contact surface areas becomes almost uniform for a volume fraction of calcite larger than 6.2%, and the contact surface areas typically range between 0 and $10,000 \mu\text{m}^2$.

From these distributions, we can compute the total surface area of contact, but also the mean contact surface area before calcification (\bar{S}_b), after calcification (\bar{S}_a) and the mean cohesive (calcite) contact surface area (\bar{S}_c) as defined in Sect. 2.3.2 (see Fig. 7). Figure 9 presents the evolution of the ratios (\bar{S}_a/\bar{S}_b) and (\bar{S}_c/\bar{S}_a) with respect to the volume fraction of calcite. The ratio (\bar{S}_a/\bar{S}_b) increases almost linearly with respect the volume fraction of calcite. For a volume fraction of calcite of 14.8%, this ratio is of the order of 6. The ratio (\bar{S}_c/\bar{S}_a) increases nonlinearly with respect to the volume fraction of calcite. This evolution shows that for a volume fraction of calcite larger than few percents (around 3%), more than 60% of the contact surface areas after biocalcification are cohesive.

3.3 Contacts orientation

Figure 10 presents the orientation of the contacts within the six samples under consideration, before and after biocalcification. In the polar representation, different colors are used to distinguish the orientation of the ‘frictional’ contacts (in blue), the ‘mixed’ contacts (in red) and the ‘cemented’ contacts (in green). The components of the fabric tensor (A^c) are also given. This figure shows that whatever the volume fraction of calcite, the orientation of the contacts is isotropic before calcification and remains isotropic after biocalcification. This latter result seems to prove that preferential direction of the flows (injection of the bacterial solution, reactants...) during the biocementation process does not induce any anisotropy. In the present case, after these injections, there is no flow through the sample. This biocementation process can be qualified as ‘static.’ In practice, if the biocementation process is applied to a dam, there is usually a continuous flow through the soil. The biocementation process is ‘dynamic,’ and in that case may lead to an anisotropic orientation of the contacts. Finally, Fig. 10 also shows that almost all the contacts which are initially frictional contacts become mixed contacts when the volume fraction of calcite is larger than few percents. This point is discussed more in details in the following section.



◀ **Fig. 7** **a** Distribution of the coordination number within the six samples, **b** distribution of the contact surface areas within the six samples, before and after biocalcification

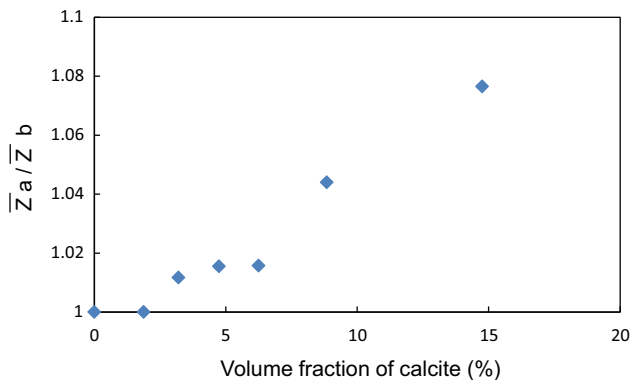


Fig. 8 Evolution of the ratio (\bar{Z}_a/\bar{Z}_b) of the mean coordination number after and before biocalcification with respect to the volume fraction of calcite

3.4 Contact types and distribution

Figure 11 presents the distribution of the different types ('frictional,' 'mixed' and 'cemented') of contact in terms of number of contact (Fig. 11a) and contact surface area (Fig. 11b) for the six samples under consideration. Figure 11a shows that, for a volume fraction of calcite of 1.9% (3% of calcite in mass), around 85% of the contacts are still 'frictional' contacts and 15% are now 'mixed' contacts. Even if the biocementation level is low, these 'mixed' contacts represent almost half of the total contact surface area within the sample. For a biocementation level of 3.2%, we can observe (Fig. 11a) that the number of frictional contacts rapidly decreases and becomes lower than 8%. Most of the contacts (around 90%) are now 'mixed' contacts and very few (around 2%) 'cemented' contacts are created. Figure 11b shows that the 'mixed' contacts represent around 98% of the total contact surface area. By increasing the level of biocementation, the number of

'frictional' of contacts still decreases and is equal to zero for the highest volume fraction of calcite, $f_c = 14.8\%$. The number of 'mixed' contacts remains the most important one, even if the number of 'cemented' contacts slightly increases. These remarks are also valid for the distributions in terms of contact surface area.

Figure 12a, b After one injection of the bacterial solution, one injection of the calcification solution leads to a small amount of calcite (around 2%); thus, most of the contacts within the sample remain 'frictional.' After the second injection of the calcification solution, most of the contacts become mixed contacts, even if the volume fraction of calcite is quite small, typically of the order of 3–4%. This second injection of the calcification solution is required in order to activate all the injected bacteria. The large number of mixed contacts created suggests that the bacteria are located in these zones, i.e., where the shear stresses induced by the flow are very small. Less than 10% of the contacts remain frictional. They are probably located in the vicinity of large pores, where high shear stresses do not allow bacteria attachment. Finally, let us remark that after this second injection of the calcification solution, the mean cohesive contact surface area represents around 60% of the mean contact surface area after calcification (see Fig. 12c).

- after one injection of the bacterial solution, one injection of the calcification solution leads to a small amount of calcite (less than 3%), and thus, most of the contacts within the sample remain 'frictional.' After the second injection of the calcification solution, most of the contacts become 'mixed' contacts, even if the volume fraction of calcite is quite small, typically of the order of 2.5–4%. This second injection of the calcification solution is required in order to activate all the injected bacteria. The large number of 'mixed' contacts created suggests that the bacteria are located in these zones, i.e., where the shear stresses induced by the flow are very small. Less than 10% of the contacts remain 'frictional.' They are probably located in the vicinity of large pores, where high shear stresses do not allow

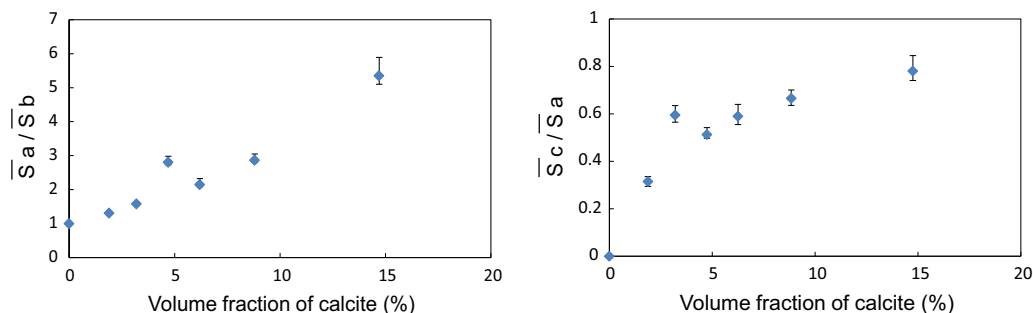
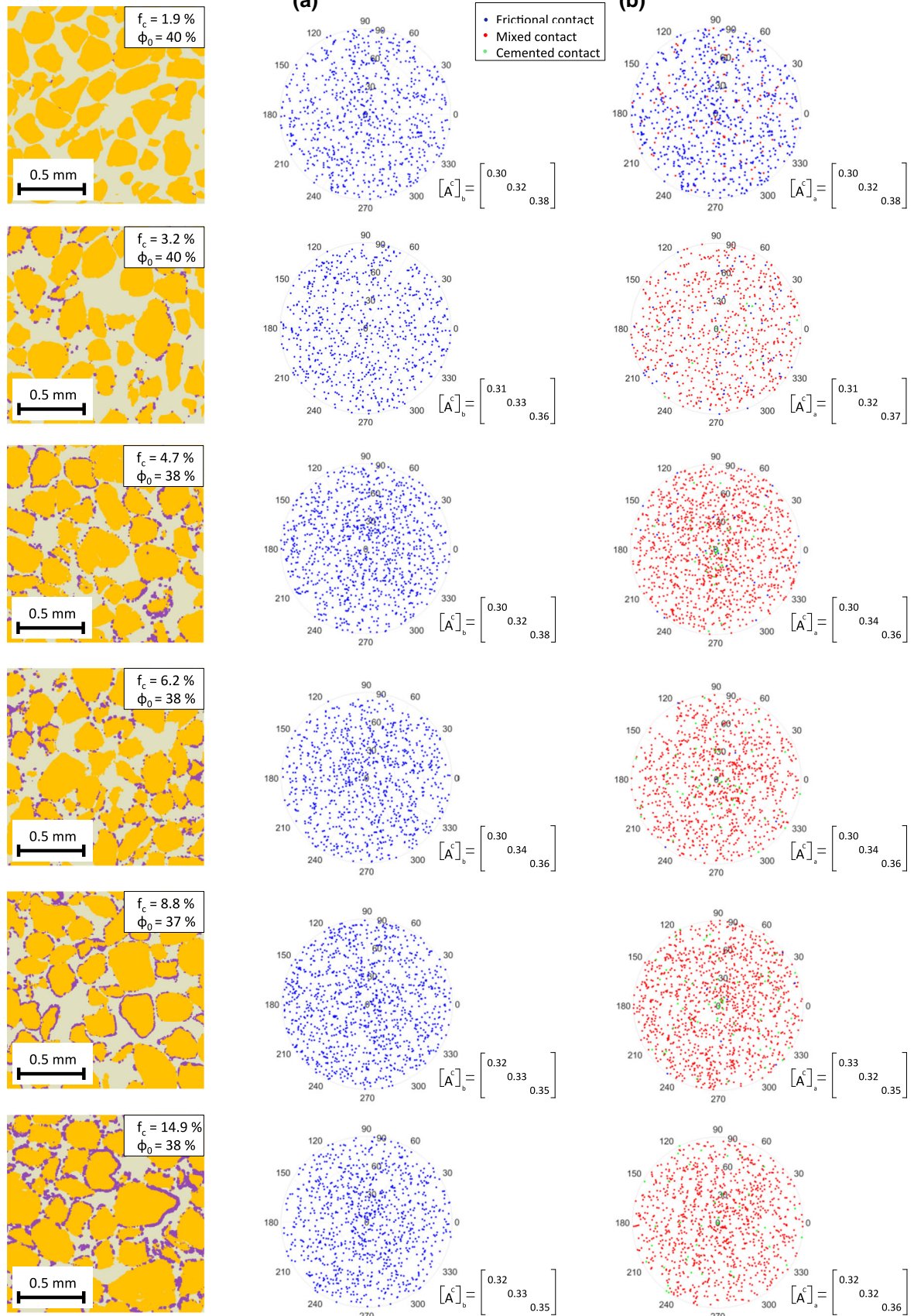


Fig. 9 Evolution of the ratios ((\bar{S}_a/\bar{S}_b) and (\bar{S}_c/\bar{S}_a) with respect to the volume fraction of calcite



◀ **Fig. 10** Orientation of the contacts within the six samples under consideration, **a** before and **b** after biocalcification

bacteria attachment. Finally, let us remark that after this second injection of the calcification solution, the mean cohesive contact surface area represents around 50% of the mean contact surface area after calcification (see Fig. 9b).

- After the second injection of the bacterial solution and the third and fourth injection of the calcification solution, the distribution of the different types of contact in terms of number or in terms of surface area remains almost the same. As expected, since the volume fraction increases, ‘frictional’ contacts disappear progressively, and the number of ‘cemented’ contacts slightly increases and represents less than 10% of the total number of contacts. This latter remark suggests that the new bacteria injected are once again attached in the zone of the initial contacts between grains, where the shear stresses are small and where grain surfaces present a high roughness created by the calcite crystals precipitated after the first injection. This is confirmed by the increase in the mean cohesive contact surface area which reaches around 80% of the mean contact surface area after calcification (see Fig. 9b).

3.5 Precipitation manner and modeling

As already discussed in the introduction, several studies have shown by simple qualitative observations (SEM, etc.) that the precipitation of calcite occurs mainly at the contacts between grains, but also on the surface of grains [9, 22, 23, 26]. According to these observations, the calcite precipitation can be seen as localized or uniform. In this section, we propose to use our results computed on 3D images in order to identify and quantify which calcite precipitation process dominates. For that purpose, in the following, we focus our attention on two microstructural properties:

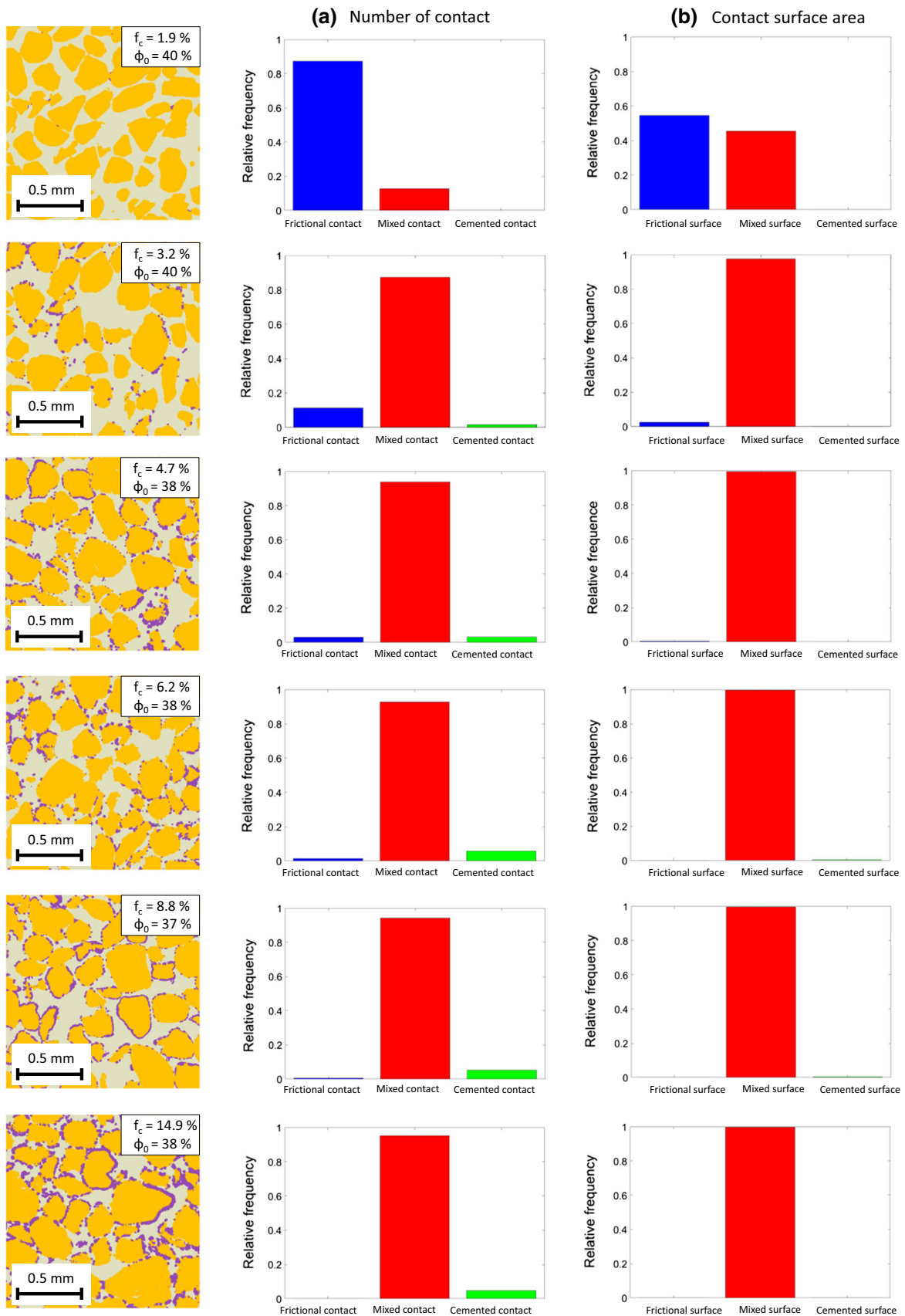
- the ratio (\bar{S}_c/\bar{S}_a) , i.e., the ratio of the mean cohesive contact surface area (\bar{S}_c) to the mean contact surface area (\bar{S}_a) after biocalcification (Fig. 15).
- the ratio (SSA_c/SSA_t) , i.e., the ratio of specific surface area of calcite (SSA_c) to the total specific surface area of the medium (SSA_t) [8]. The total specific surface area (SSA_t) is defined as $SSA_t = (S_g + S_c)/V$, where S_g and S_c are the surface area of the grain and the calcite in contact with the voids (of the air or fluid), respectively, and $V = L^3$ is the volume under consideration (Fig. 13).

The specific surface of calcite (SSA_c) is defined as $SSA_c = S_c/V$. This specific surface area of calcite characterizes the surface of calcite in contact with voids. According to the definition of SSA_c and SSA_t , we have $SSA_c/SSA_t = (S_c/S_g)/(1 + (S_c/S_g))$. This ratio, which characterizes the percentage of the initial surface of sand covered by the calcite, is equal to 0 when $S_c = 0$ (no calcite), to 0.5 when $S_c = S_g$ and 1 when $S_g = 0$, i.e., sand grains are totally covered with calcite.

Figure 13 shows the evolution of these two ratios (\bar{S}_c/\bar{S}_a) and (SSA_c/SSA_t) with respect to the volume fraction of calcite. As already underlined, the ratio (\bar{S}_c/\bar{S}_a) increases nonlinearly with respect to the volume fraction of calcite and is equal to 80% for $f_c = 14.8\%$. The ratio (SSA_c/SSA_t) also increases nonlinearly with respect to the volume fraction of calcite and tends toward an asymptotic value 0.45 (less than 45% of the sand initial surface covered by the calcite) for $f_c = 14.8\%$. The evolution of these two ratios proves that the second injection of bacteria (Fig. 12) does not increase the surface of the grain already covered by the calcite, but mainly increases the size of the contacts. It confirms that in general the calcite precipitated in the zone of contact.

In order to validate these results, they are now compared with analytical estimates assuming that the granular media are made of periodic simple cubic (SC) arrangements of grains. The initial porosity is fixed to 40%, and the diameter of grain is equal to D_{50} . Two extreme cases of precipitation are considered (Fig. 14): In the first case, we suppose that the calcite is localized at the contact and as a cylinder shape (Fig. 14a). In the second case, the grains are supposed to be covered by a uniform layer of calcite (Fig. 14b). Let us remark that in both cases (1) the coordination number is equal to 6, which is smaller to the one measured on 3D images, which ranges between 7.7 and 9.2 and (2) the creation of ‘cemented’ contacts is neglected.

Figure 15 shows the evolution of the ratios (\bar{S}_c/\bar{S}_a) and (SSA_c/SSA_t) computed on 3D images with respect to the volume fraction of calcite, in comparison with the ones derived analytically from the above simple microstructures. The numerical values of (\bar{S}_c/\bar{S}_a) lie between the two modelings (Fig. 15a). By contrast, Fig. 15b shows that the numerical values of (SSA_c/SSA_t) are in good agreement with the analytical estimates when the calcite is localized at the contacts. This comparison between our numerical results obtained on 3D images and analytical estimates confirms that the calcite is in general mainly localized at the contact between grains. Let us remark that this precipitation at the intergranular contacts can be enhanced by performing the biocementation in non-saturated conditions [6].



◀**Fig. 11** Distribution of the different types of contact, in each sample after biocementation, in terms of **a** number of contacts, **b** contacts surface area

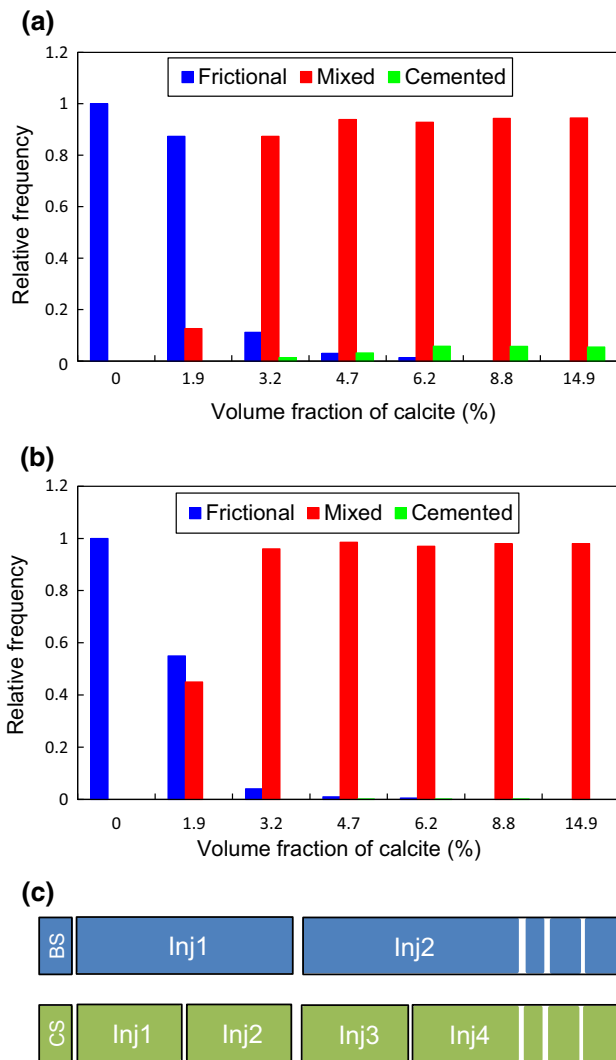


Fig. 12 Evolution of the distribution of the different types of contact with respect the volume fraction of calcite, in terms of **a** number of contacts, **b** contact surface area. **c** Typical protocol for the biocementation process: number of injections of bacterial solution (BS) and calcification solution (CS)

4 Conclusion

As underlined in the introduction, the mechanical efficiency of the biocementation process is directly related to the microstructural properties of the biocemented sand, such as the calcite volume fraction and its distribution within the pore space (localized at the contact between grains, uniform over the grain surface), the coordination number, the contact surface area, the contact orientation. In the present work, the evolution of the contact properties

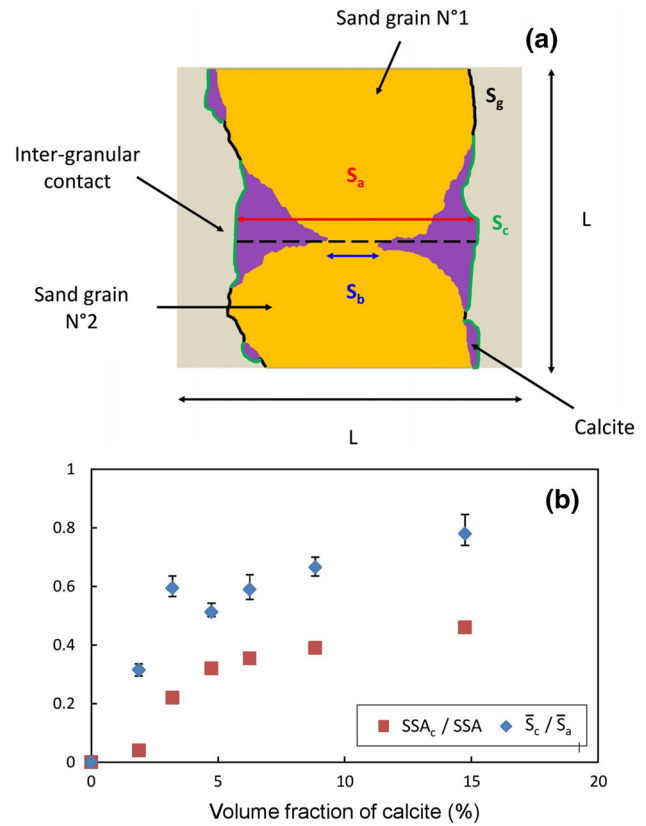


Fig. 13 **a** distribution of the calcite at the grain scale, **b** evolution of the ratio between the mean cohesive contact surface area and the mean contact surface area after calcification (\bar{S}_c/\bar{S}_a) and the ratio between the specific surface area of calcite and the total specific surface area (SSA_c/SSA_t) with the volume fraction of calcite

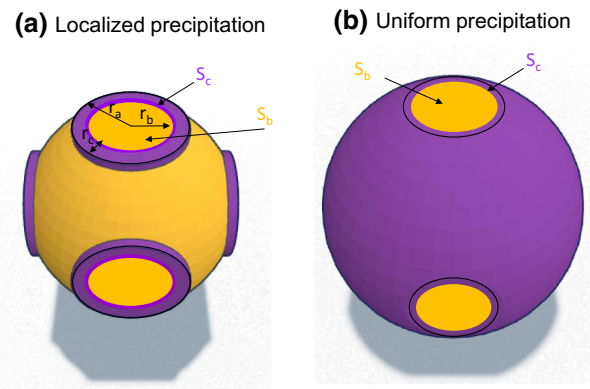


Fig. 14 Granular media is made of periodic simple cubic (SC) arrangements of grains. **a** The calcite is localized at the contact, **b** the calcification is uniform at the grain surface

(contact surfaces, coordination number, contacts orientation, type of contact, etc.) of biocemented sand as function of the cementation level ($0 < f_c < 15\%$) using 3D images obtained by X-ray micro-tomography has been determined. The obtained results point out that:

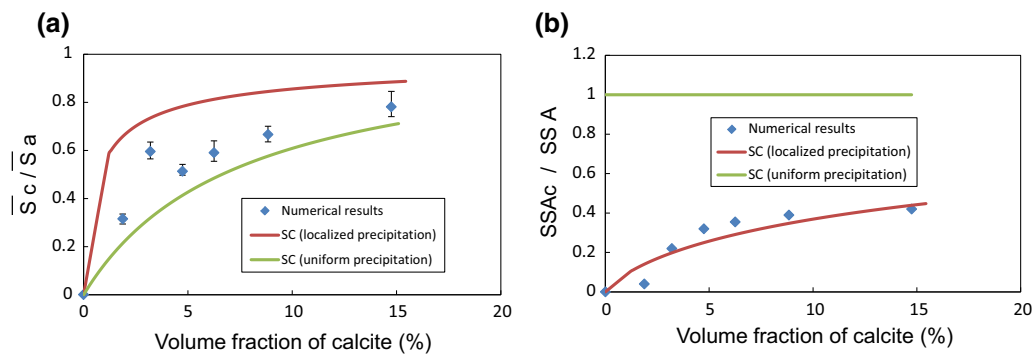


Fig. 15 Comparison between the analytical estimates and the numerical results from 3D image. **a** Evolution of the ratio (\bar{S}_c/\bar{S}_a), **b** evolution of the ratio (SSA_c/SSA_t) with respect to the volume fraction of calcite

- the coordination number, due to the creation of new contacts ('cemented' contacts), slightly increases when increasing the volume fraction of calcite. This increase is about 8% for a volume fraction of calcite of 14.8%.
- the distribution of contact surface areas changes progressively with the volume fraction of calcite (f_c). The ratio ((\bar{S}_a/\bar{S}_b)) between the mean contact surface areas after calcification ((\bar{S}_a)) and before calcification ((\bar{S}_b)) increases almost linearly with respect to the volume fraction of calcite and is the order of 6 for $f_c = 14.8\%$. By contrast, the ratio ((\bar{S}_c/\bar{S}_a)) (where \bar{S}_c is the mean cohesive contact surface area) increases nonlinearly with the volume fraction of calcite and is of the order of 60% for $f_c = 5\%$.
- the orientation of contacts within the samples is isotropic before and after calcification. This result must be put in regard to the biocementation process, which is 'static' in the present case. There is no flow through the samples after the injection of both the bacterial and calcification solutions. Probably, these observations are no more valid when a continuous flow is present during the process.
- three types of contact ('frictional,' 'mixed' and 'cemented' contacts) can be considered after biocalcification. For a volume fraction of calcite lower than 3%, most of the contacts remain 'frictional.' Beyond this value, most of the contacts (in terms of number and surface area) are 'mixed' contacts. Whatever the value of f_c , the number of new contacts ('cemented' contacts) created by the biocementation process remains quite small (less than 10% for $f_c = 14.8\%$) and the corresponding contact surface area is almost negligible. This evolution of the contacts, in terms of type, seems to be also related to the injection protocol of both the bacterial and calcification solutions.
- the precipitation of the calcite mainly occurs at the contacts between grains. Indeed, we have shown that the ratio ((\bar{S}_c/\bar{S}_a)) increases nonlinearly and tends

toward 80% for $f_c = 14.8\%$, whereas the ratio (SSA_c/SSA_t), i.e., the ratio between specific surface area of calcite (SSA_c) and the total specific surface area of the medium (SSA_t) does not exceed 45% for $f_c = 14.8\%$. These results show that the contact surface area still increases with increasing the volume fraction of calcite, whereas less than half of the surface of the grain is covered with the calcite. These results are confirmed by comparing our numerical results with analytical estimates assuming that the granular media are made of periodic simple cubic (SC) arrangements of grains and by considering two extreme cases of precipitation: (1) The calcite is localized at the contact; (2) the grains are covered by a uniform layer of calcite.

All the computed microstructural properties (coordination number, contact surface, cohesive surface, etc.) will be used in the future as input parameters in micromechanical models (DEM simulations) in order to link these microstructural properties to the macroscopic effective properties (Young modulus and shear modulus) and strength properties (cohesion and friction angle).

Acknowledgments This research is part of the BOREAL project founded under FUI 16 program and receives financial support from BPI, Metropole de Lyon and CD73. The authors acknowledge the technical support provided by Axelera Indura and all the BOREAL project partners for this research, and in particular the CNR company for funding the first author's PhD thesis. 3SR laboratory is part of the LabEx Tec 21 (Investissements d'Avenir–Grant Agreement ANR11 269 LABX0030).

References

1. Al Qabany A, Soga K (2013) Effect of chemical treatment used in MICP on engineering properties of cemented soils. *Géotechnique* 63(4):331–339
2. Al Qabany A, Soga K, Santamarina C (2012) Factors affecting efficiency of microbially induced calcite precipitation. *J Geotech Geoenviron Eng* 138(8):992–1001

3. Andò E (2013) Experimental investigation of microstructural changes in deforming granular media using x-ray tomography. Ph.D. thesis, Université Grenoble Alpes
4. Cao J, Jung J, Song X, Bate B (2018) On the soil water characteristic curves of poorly graded granular materials in aqueous polymer solutions. *Acta Geotech* 13(1):103–116
5. Chang I, Cho GC (2018) Shear strength behavior and parameters of microbial gellan gum-treated soils: from sand to clay. *Acta Geotech*. <https://doi.org/10.1007/s11440-018-0641-x>
6. Cheng L, Cord-Ruwisch R, Shahin MA (2013) Cementation of sand soil by microbially induced calcite precipitation at various degrees of saturation. *Can Geotech J* 50:81–90
7. Cui MJ, Zheng JJ, Zhang RJ, Lai HJ, Zhang J (2017) Influence of cementation level on the strength behaviour of bio-cemented sand. *Acta Geotech* 12(5):971–986
8. Dadda A, Geindreau C, Emeriault F, du Roscoat SR, Garandet A, Sapin L, Filet AE (2017) Characterization of microstructural and physical properties changes in biocemented sand using 3D X-ray microtomography. *Acta Geotech* 12(5):955–970
9. DeJong JT, Mortensen BM, Martinez BC, Nelson DC (2010) Bio-mediated soil improvement. *Ecol Eng* 36(2):197–210
10. Druckrey AM, Khalid A, Alshibli KA, Al-Raoush RI (2016) 3D characterization of sand particle-to-particle contact and morphology. *Comput Geotech* 74:26–35
11. Feng K, Montoya BM (2016) Influence of confinement and cementation level on the behavior of microbial-induced calcite precipitated Sands under monotonic drained loading. *J Geotech Geoenviron Eng* 142(1):04015057
12. Fonseca J, O'Sullivan C, Coop MR, Lee PD (2013) Quantifying the evolution of soil fabric during shearing using directional parameters. *Géotechnique* 63(6):487–499
13. Jiang NJ, Soga K (2016) The applicability of microbially induced calcite precipitation (MICP) for internal erosion control in gravel-sand mixtures. *Géotechnique* 67(1):42–55
14. Jiang NJ, Soga K, Dawoud O (2014) Experimental study of mitigation of soil internal erosion by microbially induced calcite precipitation. In: Garlangier JE, Iskander M, Hussein MH (eds) *Geo-Congress 2014*. Atlanta, Georgia, USA, February 23–26, 2014. ASCE, Reston, pp 1586–1595
15. Legland D, Kieu K, Devaux MF (2007) Computation of Minkowski measures on 2D and 3D binary images. *Image Anal Stereol* 26:83–92
16. Liu YS, Yi J, Zhang H, Zheng GQ, Paul JC (2010) Surface area estimation of digitized 3D objects using quasi-Monte Carlo methods. *Pattern Recognit* 43:3900–3909
17. Martinez B, DeJong J (2009) bio-mediated soil improvement: load transfer mechanisms at the micro- and macro- scales. In: Han J, Zheng G, Schaefer VR, Huang M (eds) *Advances in ground improvement: proceedings U.S.-China workshop on ground improvement technologies 2009*, Orlando, Florida, United States, March 14, 2009. ASCE, Reston, pp 242–251
18. Martinez B, DeJong JT, Ginn TR, Montoya BM, Barkouki TH, Hunt C, Tanyu B, Major D (2013) Experimental optimization of microbial-induced carbonate precipitation for soil improvement. *J Geotech Geoenviron Eng* 139(04):587–598
19. Montoya BM, DeJong JT, Boulanger RW (2013) Dynamic response of liquefiable sand improved by microbial-induced calcite precipitation. *Géotechnique* 63(4):302–312
20. Murtala U, Khairul AK, Kenny TPC (2016) Biological process of soil improvement in civil engineering: a review. *J Rock Mech Geotech Eng* 8:767–774
21. Otsu N (1979) A threshold selection method from gray-level histograms. *Trans Syst Man Cybern* 9(62–66):1979
22. Rong H, Li L, Qian C (2013) Influence of number of injections on mechanical properties of sandstone cemented with microbe cement. *Adv Cem Res J* 25(6):307–313
23. Sel I, Ozhan HB, Cibik R, Buyukcangaz E (2014) Bacteria-induced cementation process in loose sand medium. *Mar Georesour Geotechnol* 33(5):403–407
24. Semnani SJ, Borja RI (2017) Quantifying the heterogeneity of shale through statistical combination of imaging across scales. *Acta Geotech* 12(6):1193–1205
25. Tagliaferri F, Waller J, Andò E, Hall SA, Viggiani G, Bésuelle P, DeJong JT (2011) Observing strain localisation processes in biocemented sand using x-ray imaging. *Granul Matter* 13(3):247–250
26. Tobler DJ, Maclachlan E, Phoenix VR (2012) Microbially mediation plugging of porous media and the impact of differing injection strategies. *Ecol Eng J* 42:270–278
27. Van Paassen LA, Ghose R, Linden TJ, Van Der Star WR, Van Loosdrecht MC (2010) Quantifying biomediated ground improvement by ureolysis: large-scale biogROUT experiment. *J Geotech Geoenviron Eng* 136(12):1721–1728
28. Whiffin VS, Van Paassen LA, Harkes MP (2007) Microbial carbonate precipitation as a soil improvement technique. *Geomicrobiol J* 24(5):417–423

Publisher's Note Springer Nature remains neutral with regard to jurisdictional claims in published maps and institutional affiliations.